ACS APPLIED MATERIALS & INTERFACES

Research Article

www.acsami.org

Self-Powered UV Photosensor Based on PEDOT:PSS/ZnO Micro/Nanowire with Strain-Modulated Photoresponse

Pei Lin,[†] Xiaoqin Yan,[†] Zheng Zhang,[†] Yanwei Shen,[†] Yanguang Zhao,[†] Zhiming Bai,[†] and Yue Zhang[†,‡,*]

[†]State Key Laboratory for Advanced Metals and Materials, School of Materials Science and Engineering, [‡]Key Laboratory of New Energy Materials and Technologies, University of Science and Technology Beijing, Beijing 100083, People's Republic of China.

ABSTRACT: Developing tailored micro/nanostructure interfaces is an effective way to make novel optoelectronic devices or enhance their performances. Here we report the fabrication of a PEDOT:PSS/ZnO micro/nanowire-based self-powered UV photosensor. The generation of photocurrent at zero bias is attributed to the separation of photogenerated electron−hole pairs within the built-in electric field at the PEDOT:PSS/ZnO interface upon UV light illumination. Furthermore, the piezotronic effect on the UV photoresponsivity under different strains is investigated, which is due to the modification of energy band diagram at the p−n heterojunction by strain-induced piezoelectric polarization. This study demonstrates a prospective approach to engineering the performance of a photodetector through straining and may offer theoretical supporting in future optoelectronic device fabrication and modification.

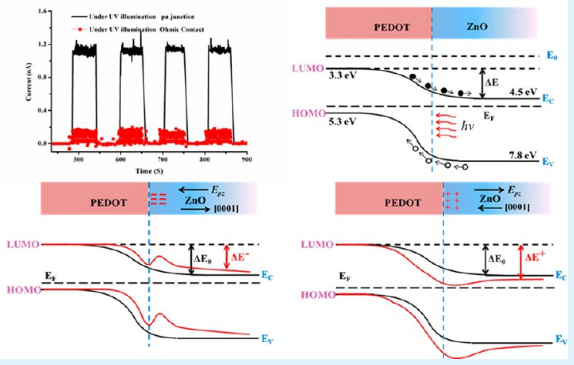

KEYWORDS: *self-powered, UV photodetector, p−n junction, interface modulation, strain*

INTRODUCTION

Interfaces are essential component for fabricating electronic, optoelectronic, and electromechanical devices.[1] Most of the time, the modern nanoelectronics rely to a large degree on the properties of interfaces between two heterostructured semiconductors. Thus, the ability to precisely tailor interfaces provides a wealth of possibilities to enhance the performance or introduce completely novel functionality.[2,3] The research field of interface engineering is therefore drawing more and more attention to rationally design heterostructures and make use of the engineered interface property to fabricate devices.[4] So far, multiple approaches have been introduced to manipulate the features of interfaces. By electrochemically altering the work function of the polymer poly-(pyrrole), contact barrier modulation in poly-(pyrrole)/n-InP Schottky diode was realized.[5] More recently, active control of the built-in potential in a carbon nanotube/semiconductor junction solar cell was also possible.[6] But the complicated fabrication process and device configuration may hinder their applications in practical working conditions.

Due to the coupled piezoelectric and semiconducting properties, the ZnO nanomaterial is recognized as promising building blocks for future electronic, optoelectronic and electromechanical devices.[7−9] When the ZnO nanocrystal is subjected to mechanical deformation, a piezopotential is created due to the polarization of ions. By taking advantage of this strain-induced piezoelectric polarization, the charge carrier transport behavior across a Schottky interface or p−n junction could be effectively tuned.[7] Making use of the piezotronic effect to boost the device performance has also been demonstrated, such as metal-semiconductor-metal (M-S-M) structured photosensors,[10−12] light-emitting diodes,[13] micro/nanowire solar cells,[14] and photocells.[15]

Nowadays, self-powered nanosensors and nanosystems is another attractive theme that can greatly enhance the adaptability and sustainability of such devices.[16−19] In this paper, an approach of fabricating batteryless flexible UV photosensor based on PEDOT:PSS/ZnO micro/nanowire was demonstrated. The device shows excellent photosensing properties under UV light illumination at zero bias with a fast response time. Meanwhile, the piezotronic effect on the UV photoresponsivity under different strains is also investigated, which is attributed to modification of energy band diagram at the p−n junction by piezopotential. The fabrication of such devices has the merits of low cost, simplicity, and may have potential applications in fields such as medicine, communication and environmental monitoring.

EXPERIMENTAL SECTION

ZnO micro/nanowires investigated in this work were prepared by a chemical vapor deposition (CVD) method as reported previously.[20] For easy manipulation and device fabrication, ZnO wires with diameter of several micrometers and length of hundreds of micrometers were chosen, but the same methodology and fabrication process apply to nanowires.[21] After dispersion in ethanol, ZnO wires of interest were transferred onto a flexible polystyrene (PS) substrate with 40 mm length, 10 mm width, and 0.4 mm thickness. To avoid the

Received: January 15, 2013
Accepted: March 26, 2013
Published: March 26, 2013

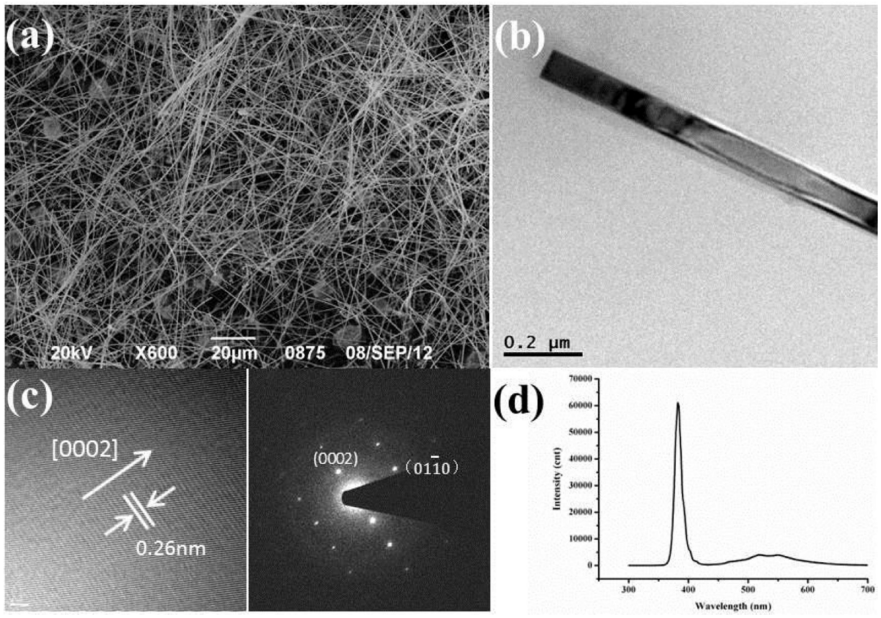

Figure 1. (a) SEM image of the as-prepared ZnO micro/nanowires. (b) Low-magnification TEM image of the ZnO wire. (c) HRTEM image and the corresponding SAED pattern. (d) Photoluminescence spectrum of ZnO micro/nanowires with an excitation wavelength of 325 nm.

movement of ZnO wire and eliminate the possible PEDOT:PSS/ZnO contact area change during device fabrication and test procedure, the bottom at one end of ZnO wire was fixed by a thin film of epoxy.[13] Then, PEDOT:PSS was dropped on the fixed end to form p−n junction and silver paste was applied to the other end as an electrode. After that, the whole device was packaged with a thin layer of poly (dimethylsiloxane) (PDMS) to keep it from contamination and moisture.[21] The morphology and structure of the ZnO wire and the fabricated devices were characterized by optical microscope, scanning electron microscope (FE-SEM, LEO1530) and transmission electron microscope (JEOL, JEM-2010). The photoluminescence spectrum was performed to evaluate the crystalline property by using a continuous He−Cd (325 nm) laser as an excitation source. The room temperature electrical transport characteristic and the photoresponse property were recorded with a semiconductor analysis system (Keithley 4200).

RESULTS AND DISCUSSION

The typical top-view scanning electron microscopy (SEM) image of the as-synthesized ZnO micro/nanowires is presented in Figure 1a, with a lengths of about hundreds of micrometers and diameters from hundreds of nanometers to several micrometers. Figure 1b depicts the low-magnification TEM image of ZnO wire. HRTEM image and the corresponding select-area electron diffraction (SAED) pattern were shown in Figure 1c, which indicate that the micro/nanowire is a wurtzite structured single crystal, growing dominantly in [0001] direction. Figure 1d illustrates the room-temperature photoluminescence spectrum with an excitation wavelength of 325 nm. The relatively strong UV emission at about 380 nm and the negligible deep-level emission at about 520 nm indicate that the as-prepared ZnO micro/nanowires have good crystallinity and low concentration of defects.[22] It can be perceived that the synthesized micro/nanowires are appropriate for device fabrication and investigation of the piezotronic effect.[23]

The schematic of the fabricated device provided in a and b Figure 2 shows the optical image of it. It is straightforward to see that the $I-V$ characteristic of PEDOT:PSS/ZnO/Ag heterojunctions display a significant diode-like behavior with relatively low reverse leakage current of 10^{-12} A at a reverse bias of −3.0 V, as shown in Figure 2c. The current rectification ratio

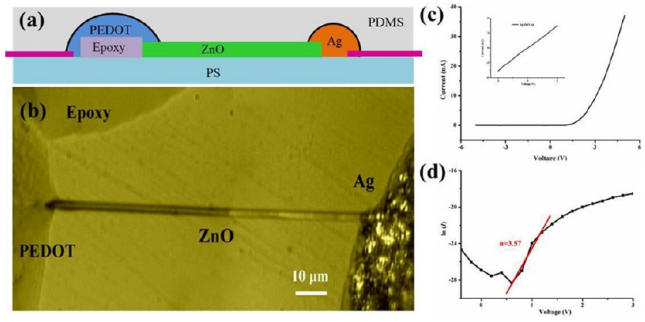

Figure 2. (a) Schematic of the fabricated device. (b) Optical image of the fabricated device. (c) $I-V$ characteristic of a PEDOT:PSS/ZnO/Ag heterojunctions. The inset shows the $I-V$ characteristic of Ag-ZnO-Ag. (d) Semi-logarithmic plot of current and voltage for the fabricated PEDOT:PSS/ZnO/Ag heterojunctions.

can be obtained to be about 3×10^3 at ±3 V.To confirm that the observed nonlinearity is due to the formation of p−n junction at the PEDOT:PSS/ZnO interface, we measured $I-V$ characteristic of Ag-ZnO-Ag, as indicated in the inset of Figure 2c. The work function of Ag ($\Phi_{Ag} \approx 4.26$ eV) is not much different from the electron affinity of ZnO ($\Phi_{ZnO} \approx 4.5$ eV), leading to the formation of both Ohmic contacts at the two ends.[18]

To further analyze the property of the fabricated p−n junction, thermionic emission model was applied to describe the electrical transport of PEDOT:PSS/ZnO heterojunction when forward voltage $V \gg 3kT/q$. According to this model, the $I-V$ characteristic under forward bias can be expressed as[24]

$$I = I_0\left[\exp\frac{qV}{nKT} - 1\right] \quad (1)$$

Where I_0 is the reverse saturation current, q is the elementary charge, V is the forward biasing voltage, K is the Boltzmann constant, n is the ideality factor, and T is the absolute temperature. The reverse saturation current I_0 is expressed as

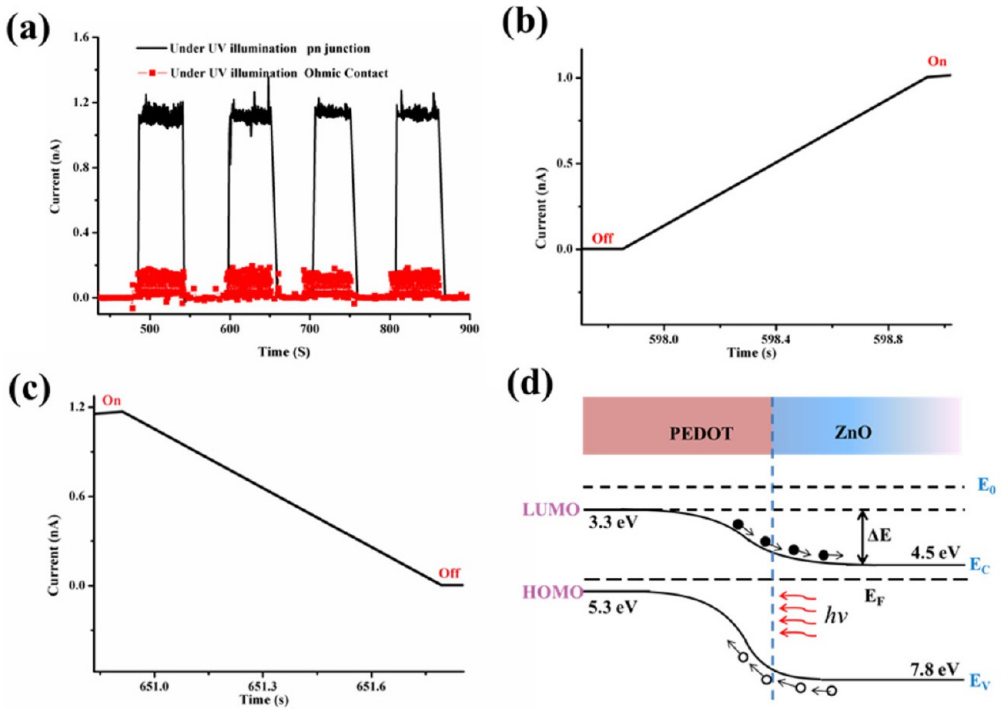

Figure 3. (a) Photoresponse comparison of PEDOT:PSS/ZnO heterojunction and Ag-ZnO-Ag Ohmic contact, which is shown using black and red curves respectively. (b, c) Enlarged parts of the current response, showing the corresponding rise and decay time. (d) Energy band diagram of PEDOT:PSS/ZnO heterojunction under light illumination, ΔE corresponds to the built-in potential.

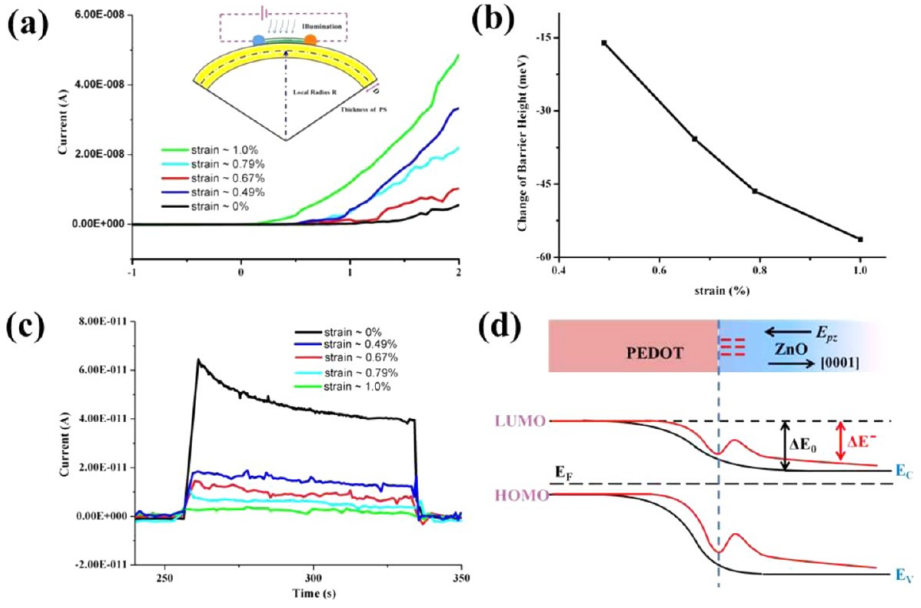

Figure 4. (a) Typical $I-V$ characteristics of the device under different strains. The inset shows the cross-sectional schematic of strain-dependent electrical measurement system. (b) Derived barrier height change of PEDOT:PSS/ZnO heterojunction as a function of strains. (c) Time-resolved characteristic of the UV response with different strains. (d) Schematic energy band diagram of PEDOT:PSS/ZnO heterojunction with and without the presence of strain, shown in red and black curves, respectively.

$$I_0 = AA^*T^2\exp\left(\frac{-q\Phi_b}{KT}\right) \quad (2)$$

where A is the junction area, A^* is the effective Richardson constant, and Φ_b is the junction barrier height.

Through linearly fitting the semi logarithmic plot of current and voltage as depicted in Figure 2(d), the ideality factor n = 3.57 could be obtained from the slope. For an ideal p−n junction, the ideality factor n should be 1 at low forward bias.[24] Here, the deviation of n from the ideal one is probably due to the presence of surface states, which provide multiple current pathways between the heterointerface.[25]

Performances of the photodetector were initially measured in the atmospheric environment without strain. In Figure 3a, the black curve represents the time-resolved UV photoresponse of the fabricated device at zero-voltage bias. A relatively low dark

dx.doi.org/10.1021/am4008775 | ACS Appl. Mater. Interfaces 2013, 5, 3671−3676

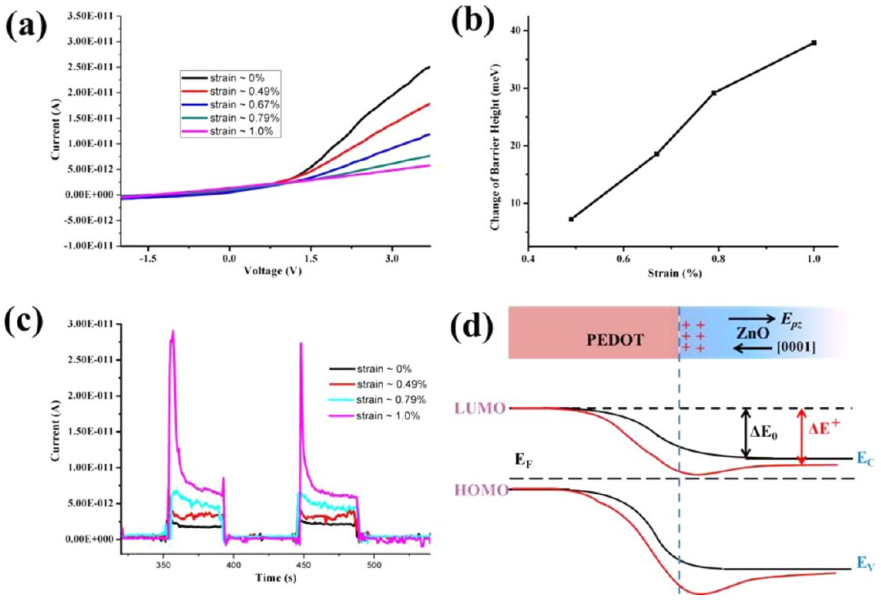

Figure 5. (a) Typical $I-V$ characteristics of the device under different strains. (b) Calculated barrier height change of PEDOT:PSS/ZnO heterojunction as a function of strain. (c) Time-resolved characteristic of UV response with different strains. (d) Schematic energy band structure of PEDOT:PSS/ZnO heterojunction with and without the presence of strain, shown in red and black curves, respectively.

current of <1 pA could be observed and the photocurrent was about 1 nA when the light illumination was on. The sensitivity of the device, defined as $(I_{light} - I_{dark})/I_{dark}$ was found to be about 1×10^3. For all we know, the photocurrent may result from the micro/nanowire because of its photoconductive behavior.[26,27] Thus, control experiment was carried out using Ag-ZnO-Ag Ohmic contact device. As the red curve shown in Figure 3a, when the device was illuminated under UV light at zero bias, only random noise signal could be observed. These results verified that the presence of PEDOT:PSS/ZnO is therefore the essential component of our self-powered photosensors. The corresponding rise and decay time of the fabricated device are shown in panels b and c in Figure 3, and are both less than 1 s. Compared with the traditional micro/nanowire photodetector based on the photoconductivity effect, this self-powered photosensor possesses faster photoresponse speed due to the absence of surface oxygen adsorption and desorption process.[28−31] Considering the time-resolution of the testing instrument and the setting parameters, the response time could be much shorter.

This self-powered phenomenon in such device can be understood based on their energy band diagram and the principle of photovoltaic effect.[32,33] When the PEDOT:PSS and ZnO contact in the dark, electron transfer occurs across the interface from ZnO to PEDOT:PSS and holes in the opposite direction until their Fermi levels become aligned, resulting the formation of a built-in potential ΔE and thus the band bending at the interface, as shown in Figure 3d. When the junction is illuminated by UV light (325 nm), photoexcited electrons and holes formed. Under the built-in electric field force, photogenerated electron−hole pairs will be separated toward opposite direction, which results in the generation of photocurrent.[34,35] Furthermore, the photocurrent due to the photovoltaic effect can be generated repeatedly.

To further investigate the strain effects on UV sensing properties, $I-V$ characteristic of the fabricated device was measured under various apparent tensile strains. Because the piezopotential is related with the pointing direction of +c-axis, there are two different ways to contact PEDOT:PSS with ZnO micro/nanowire during the device fabrication procedure.[13] The first way is that the [0001] direction points from the PEDOT:PSS to ZnO. By applying different bending curvatures, the strain could be calculated using the local radius R and the thickness of PS substrate D as[36]

$$\varepsilon = \pm\frac{D}{2R} \tag{3}$$

Because the size of substrate is much larger than that of ZnO micro/nanowire, it can be regarded as being subjected to a pure tensile strain under such condition.[15] The inset of Figure 4a illustrates the cross-sectional schematic of strain-dependent electrical measurement system. As shown in Figure 4a, the $I-V$ curves shift upward, along with the decrease of threshold voltage with increased strains. According to the aforementioned thermionic emission model and assuming that the contact area A, the effective Richardson constant A^*, and impurity density are independent of strain, the change of barrier height $\Delta\Phi_b$ could be derived as

$$\ln[I(\varepsilon)/I(0)] = -q\Delta\Phi_b/KT \tag{4}$$

Where $I(\varepsilon)$ and $I(0)$ are the currents measured at fixed bias with and without strain. The results are extracted and plotted in Figure 4b, indicating that the barrier height of heterojunction decreases with the increased tensile strains.

Figure 4c depicts the time-resolved characteristic of UV response with and without strain at zero bias. It is noted that the photocurrent along with the sensitivity decreased step by step when gradually increase the applied tensile strains, whereas the response time remains almost unchanged. The schematic energy band diagram is shown in Figure 4d to illustrate this phenomenon. When the +c-axis points from PEDOT:PSS to ZnO and tensile strain was applied to the ZnO wire, a negative piezopotential is created at the PEDOT:PSS/ZnO interface, which raised the energy of the electrons in the conduction band. Therefore, The energy band difference between the conduction band of ZnO and the lowest unoccupied molecular

orbit (LUMO) of PEDOT:PSS would be reduced and the barrier height became lower.[13] The decreased barrier height weakened the strength of built-in electric field. Therefore, the recombination of photogenerated electron−hole pairs could be enhanced, and the photocurrent decreased.

The other contact way between the PEDOT and ZnO micro/nanowire is that the +*c*-axis points from ZnO to PEDOT:PSS. In this instance, a positive piezopotential would be created at the heterojunction interface when tensile strain was applied. As shown in Figure 5a, the current decreased, along with the increase of threshold voltage with the increased strain. The calculated change of barrier height is plotted in Figure 5b, it can be obtained that the barrier height of p−n junction increases with increased tensile strains. The time-resolved photoresponse at zero-voltage bias of such device is presented in Figure 5c with the UV illumination switching on and off. It can be seen that the photocurrent and the corresponding sensitivity increase with increasing the applied strains, whereas the response time remained constant.

This phenomenon could be explained from the schematic of energy band profile as shown in Figure 5d. Because of the [0001] direction pointing from ZnO to PEDOT, a positive piezopotential was established at the interface. The positive potential lowered the conduction band energy of ZnO, therefore the barrier height increased. The increased barrier height will induce the broadening of the space-charge region and the strengthening of the built-in electric field.[33] As a result, the photogenerated electron−hole pairs could be separated and transport more efficiently, giving rise to the enhanced photocurrent and sensitivity.

It should be mentioned that our work focused on the demonstration of manipulating the interface features through straining and then modulating the properties of photodetector, the constructed devices were no further optimized. For the practical application, there is a plenty of room to further improve its performance through additional optimization process of the device configuration and the heterointerface.[37] Furthermore, the property of self-power might make it more suitable to work sustainably and adaptively.

CONCLUSION

In summary, on the basis of the property of PEDOT:PSS/ZnO micro/nanowire heterojunction, a self-powered UV photodetector was fabricated. At zero bias, the sensitivity of device was about 10^3 under the illumination of UV light (325 nm), along with a fast response time <1 s. The property of self-power is attributed to the formation of built-in electric field at the heterojunction, under which the photogenerated carriers was separated toward opposite directions. Due to the intrinsic coupled semiconducting and piezoelectric properties of ZnO, the strain-induced piezopotential could tune the energy band profile at the heterointerface and increase/decrease the barrier height, consequently modulate the performance of these optoelectronic devices. Compared with traditional ones, these flexible self-powered photosensors are probable to work in harsh environment more sustainably and independently. This unique property might expand its applications in medicine, communication, and environmental monitoring areas.

AUTHOR INFORMATION

Corresponding Author

*Tel:+86-010-62333113. E-mail: yuezhang@ustb.edu.cn.

Notes

The authors declare no competing financial interest.

ACKNOWLEDGMENTS

This work was supported by the National Major Research Program of China (2013CB932602), Major Project of International Cooperation and Exchanges (2012DFA50990), NSFC (51232001, 51172022, 50972011), the Research Fund of Co-construction Program from Beijing Municipal Commission of Education, the Fundamental Research Funds for the Central Universities, the Program for Changjiang Scholars and Innovative Research Team in University, the Beijing Novel Program (2008B19), and the Program for New Century Excellent Talents (NCET-09-0219).

REFERENCES

(1) Shi, J.; Starr, M. B.; Xiang, H.; Hara, Y.; Anderson, M. A.; Seo, J.-H.; Ma, Z.; Wang, X. *Nano Lett.* **2011**, *11*, 5587.
(2) Mannhart, J.; Schlom, D. G. *Science* **2010**, *327*, 1607.
(3) Chakhalian, J.; Freeland, J. W.; Habermeier, H.-U.; Cristiani, G.; Khaliullin, G.; van Veenendaal, M.; Keimer, B. *Science* **2007**, *318*, 1114.
(4) Shi, J.; Starr, M. B.; Wang, X. *Adv. Mater.* **2012**, *24*, 4683.
(5) Lonergan, M. C. *Science* **1997**, *278*, 2103.
(6) Wadhwa, P.; Liu, B.; McCarthy, M. A.; Wu, Z.; Rinzler, A. G. *Nano Lett.* **2010**, *10*, 5001.
(7) Wang, Z. L. *Adv. Mater.* **2012**, *24*, 4632.
(8) Espinosa, H. D.; Bernal, R. A.; Minary-Jolandan, M. *Adv. Mater.* **2012**, *24*, 4656.
(9) Zhang, Y.; Yan, X.; Yang, Y.; Huang, Y.; Liao, Q.; Qi, J. *Adv. Mater.* **2012**, *24*, 4647.
(10) Yang, Q.; Guo, X.; Wang, W.; Zhang, Y.; Xu, S.; Lien, D. H.; Wang, Z. L. *ACS Nano* **2010**, *4*, 6285.
(11) Guo, W.; Yang, Y.; Qi, J.; Zhao, J.; Zhang, Y. *Appl. Phys. Lett.* **2010**, *97*, 133112.
(12) Wang, R.-C.; Lin, H.-Y.; Wang, C.-H.; Liu, C.-P. *Adv. Funct. Mater.* **2012**, *22*, 3875.
(13) Yang, Q.; Wang, W.; Xu, S.; Wang, Z. L. *Nano Lett.* **2011**, *11*, 4012.
(14) Yang, Y.; Guo, W.; Zhang, Y.; Ding, Y.; Wang, X.; Wang, Z. L. *Nano Lett.* **2011**, *11*, 4812.
(15) Hu, Y.; Zhang, Y.; Chang, Y.; Snyder, R. L.; Wang, Z. L. *ACS Nano* **2010**, *4*, 4220.
(16) Wang, Z. L. *Adv. Mater.* **2012**, *24*, 280.
(17) Wang, X.; Wang, Y.; Åberg, D.; Erhart, P.; Misra, N.; Noy, A.; Hamza, A. V.; Yang, J. *Adv. Mater.* **2011**, *23*, 117.
(18) Yang, Y.; Guo, W.; Qi, J.; Zhao, J.; Zhang, Y. *Appl. Phys. Lett.* **2010**, *97*, 223113.
(19) Bai, Z.; Yan, X.; Chen, X.; Liu, H.; Shen, Y.; Zhang, Y. *Curr. Appl. Phys.* **2013**, *13*, 165.
(20) Huang, Y. H.; Zhang, Y.; Liu, L.; Fan, S. S.; Wei, Y.; He, J. *J. Nanosci. Nanotechnol.* **2006**, *6*, 787.
(21) Zhou, J.; Gu, Y.; Fei, P.; Mai, W.; Gao, Y.; Yang, R.; Bao, G.; Wang, Z. L. *Nano Lett.* **2008**, *8*, 3035.
(22) Shalish, I.; Temkin, H.; Narayanamurti, V. *Phys. Rev. B* **2004**, *69*, 245401.
(23) Hansen, B. J.; Liu, Y.; Yang, R.; Wang, Z. L. *ACS Nano* **2010**, *4*, 3647.
(24) Sharma, B. K.; Khare, N.; Ahmad, S. *Solid State Commun.* **2009**, *149*, 771.
(25) Wright, J. S.; Khanna, R.; Voss, L. F.; Stafford, L.; Gila, B. P.; Norton, D. P.; Pearton, S. J.; Wang, H. T.; Jang, S.; Anderson, T.; Chen, J. J.; Kang, B. S.; Ren, F.; Shen, H.; LaRoche, J. R.; Ip, K. *Appl. Surf. Sci.* **2007**, *253*, 3766.
(26) Tang, Y. B.; Chen, Z. H.; Song, H. S.; Lee, C. S.; Cong, H. T.; Cheng, H. M.; Zhang, W. J.; Bello, I.; Lee, S. T. *Nano Lett.* **2008**, *8*, 4191.
(27) Baxter, J. B.; Aydil, E. S. *Appl. Phys. Lett.* **2005**, *86*, 053114.

(28) Bie, Y.-Q.; Liao, Z.-M.; Zhang, H.-Z.; Li, G.-R.; Ye, Y.; Zhou, Y.-B.; Xu, J.; Qin, Z.-X.; Dai, L.; Yu, D.-P. *Adv. Mater.* **2011**, *23*, 649.
(29) Ates, E. S.; Kucukyildiz, S.; Unalan, H. E. *ACS Appl. Mater. Interfaces* **2012**, *4*, 5142.
(30) Zhao, Y.; Zhang, J.; Jiang, D.; Shan, C.; Zhang, Z.; Yao, B.; Zhao, D.; Shen, D. *ACS Appl. Mater. Interfaces* **2009**, *1*, 2428.
(31) Yan, C.; Singh, N.; Cai, H.; Gan, C. L.; Lee, P. S. *ACS Appl. Mater. Interfaces* **2010**, *2*, 1794.
(32) Liao, Z.-M.; Xu, J.; Zhang, J.-M.; Yu, D.-P. *Appl. Phys. Lett.* **2008**, *93*, 023111.
(33) Ye, Y.; Dai, L.; Wu, P. C.; Liu, C.; Sun, T.; Ma, R. M.; Qin, G. G. *Nanotechnology* **2009**, *20*, 375202.
(34) Xie, C.; Lv, P.; Nie, B.; Jie, J.; Zhang, X.; Wang, Z.; Jiang, P.; Hu, Z.; Luo, L.; Zhu, Z.; Wang, L.; Wu, C. *Appl. Phys. Lett.* **2011**, *99*, 133113.
(35) Li, L.; Wang, H. Q.; Fang, X. S.; Zhai, T. Y.; Bando, Y.; Golberg, D. *Energy Environ. Sci.* **2011**, *4*, 2586.
(36) Yang, R.; Qin, Y.; Dai, L.; Wang, Z. L. *Nat. Nanotechnol.* **2009**, *4*, 34.
(37) Chung, D. S.; Rho, Y.; Ree, M.; Kwon, S.-K.; Kim, Y.-H. *ACS Appl. Mater. Interfaces* **2012**, *4*, 4758.